ISSN: 1410-8917
e-ISSN: 2597-9914

Jurnal Kimia Sains dan Aplikasi 28 (9) (2025): 488-501

Jurnal Kimia Sains dan Aplikasi
Journal of Scientific and Applied Chemistry

Journal homepage: http://ejournal.undip.ac.id/index.php/ksa

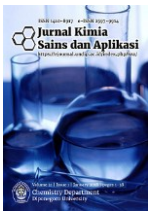

Chitosan-Impregnated Activated Carbon Derived from Sugarcane Bagasse for Alizarin Red S Adsorption

Dina Fitriana [1,*], Sri Hastuti [1], Abu Masykur [1], Atmanto Heru Wibowo [1], Puput Nursetyani [1], Miftahul Rohmah [1], Faiza Dzikra Az-Zahra [1]

[1] Chemistry Department, Faculty of Mathematics and Natural Sciences, Universitas Sebelas Maret, Jl. Ir. Sutami 36A, Kentingan, Surakarta, 57126, Indonesia

* Corresponding author: dina.fitriana@staff.uns.ac.id

https://doi.org/10.14710/jksa.28.9.488-501

Article Info

Article history:

Received: 08th June 2025
Revised: 01st November 2025
Accepted: 05th November 2025
Online: 08th December 2025

Keywords:
adsorption; alizarin red; activated carbon; sugarcane bagasse; chitosan

Abstract

In the present study, a chitosan-impregnated activated carbon derived from sugarcane bagasse (Cs-Act SB) has been synthesized for the removal of Alizarin Red S (ARS) dye from an aqueous solution. The dried sugarcane bagasse sample was rinsed with 0.5% HCl to eliminate impurities and subsequently dried overnight at 110°C. Thereafter, it was subjected to carbonization in a furnace at 600°C for 2 h to produce sugarcane bagasse biochar (SB). The SB was then chemically activated using NaOH and physically activated in a muffle furnace at 750°C for 2 h to produce activated carbon (Act-SB). The obtained Act-SB was then modified using chitosan to yield Cs-Act SB biocomposite. The Act-SB and Cs-Act SB were characterized based on moisture content and ash content, pH points of zero charge (pH_{PZC}), FT-IR, SEM-EDX, and TGA-DTA analysis. The Cs-Act SB has a moisture content of 4.0% and an ash content of 3.40%, respectively. The results show that the adsorbent process is desirable at low pH under acidic conditions (pH 2) with a pH_{PZC} of 4.58. Based on the FT-IR spectra, the characteristic peaks of the chitosan were shown for Cs-Act SB at 3440 cm^{-1} due to the stretching vibration of the hydroxyl and amino functional group. The surface of Cs-Act SB has an irregular and heterogeneous surface and has high carbon content (84.42%). The TGA-DTA results showed the stability of Cs-Act SB with respect to temperature. Moreover, the adsorption kinetics were found to follow a pseudo-second-order kinetic model, and the adsorption isotherms are best described by the Langmuir model for both Act-SB and Cs-Act SB. The determined Langmuir maximum adsorption capacity of Cs-Act SB and Act-SB for the ARS dye adsorption were 78.13 mg g^{-1} and 30.03 mg g^{-1}, respectively. Kinetics and adsorption isotherm studies suggest that the capacity, equilibrium constant, and energy of the Cs-Act SB in adsorbing ARS dye are improved compared to Act-SB.

1. Introduction

Alizarin Red S (ARS), also known as 1,2-dihydroxy-9,10-anthraquinonesulfonicacid is a water-soluble anthraquinone dye synthesized by sulfonation of alizarin. It has been widely used in textile dyeing [1], acid-base indicator (pKa 4.6 – 6.5) that exhibits a distinct color change from yellow to purple in the pH range of 2-12 [2], and biological staining [3].

ARS is an extremely persistent anthraquinone dye that cannot be completely degraded by general chemical, physical, and biological processes. Due to its aromatic amine groups, ARS has high physicochemical stability and photothermal stability, which makes it resistant to biodegradation [4, 5]. The toxicity and carcinogenic effects of these persistent and non-biodegradable pollutants are widely known [6]. Despite the excessive use of ARS at the commercial scale, the accumulation of this particular dye in water sources poses severe health risks to both the aquatic ecosystem and humans, including irritations that can cause harm to the eyes, skin, and respiratory system [7].

Numerous techniques have been employed to eliminate dyes from wastewater, such as ion-exchange [8], precipitation [9], membrane-based separation [10], electrochemical degradation [11], advanced oxidation process [12], ultrafiltration [13], and catalytic ozonation [14]. Among these techniques, adsorption stands out as the most commonly used method of dye removal that has significant advantages, including its versatility, simple design and operation, cost-effectiveness, efficient regeneration, and environmentally friendly adsorbents [15, 16, 17].

In recent years, numerous research studies have focused on the sustainable development of eco-friendly adsorbents for water treatment. The development of activated carbon derived from agricultural waste, particularly lignocellulosic materials, has been studied. Utilizing agricultural waste for activated carbon production addresses waste disposal issues, provides a sustainable method for producing high-value adsorbents, and offers a low-cost alternative that makes them economically viable for large-scale applications [18, 19].

One agro-industrial waste that is abundant in Indonesia is sugarcane bagasse. Due to its high organic carbon content, it may be used as a feedstock to produce activated carbon. The raw sugarcane bagasse is mainly composed of cellulose (45–55 wt%), hemicellulose (20–25 wt%), and lignin (18–24 wt%) [20]. This lignocellulosic structure provides a natural framework for adsorption due to its porous nature and high surface area [21].

However, the primary drawback of raw sugarcane bagasse biochar is that it has a negatively charged surface, which reduces its effectiveness, particularly when it comes to the adsorption of ARS and other anionic pollutants [22]. Consequently, a variety of modifications, particularly those involving metal or metal oxide impregnation, have been noticed to increase the adsorption capacity of biochar.

Although metal impregnation has been found to increase the adsorption capacity of sugarcane bagasse biochar, the majority of metals are poisonous; therefore, additional treatment is required before the saturated biosorbent may be disposed of in the environment [22]. In this article, we described an alternative method for modifying sugarcane bagasse biochar that may also be used to remove ARS anionic dye from aqueous solution.

Chitosan is one of the most often utilized biomolecules in the adsorption of various water pollutants due to its numerous superior properties, including its adsorption capacity, biodegradability, and biocompatibility [23]. It is a cationic biopolymer derived from chitin, which is known for its high adsorption capacity due to the presence of amino ($-NH_2$) and hydroxyl groups (OH^-) [24]. In wastewater treatment methods, these groups are considered active adsorbent sites for eliminating specific contaminants, including heavy metals and synthetic dyes. Furthermore, the amine functional groups in chitosan may interact with different kinds of contaminants in an aqueous solution because they can transform into a polyelectrolyte with positively charged ions, particularly in acidic environments [25].

Scientists have recently developed biocomposites from biomass that are more effective at removing pollutants and dyes from water than raw biomass. This is achieved through chemical pretreatment, increased surface area, enhanced functional groups, and the development of composite materials, making them highly effective for wastewater treatment applications [20].

In this study, we developed an eco-friendly, high-performance adsorbent derived from sugarcane bagasse and modified with the chitosan biopolymer to enhance the removal of the ARS anionic dye. The composite in this work was synthesized under mild conditions. Furthermore, the use of locally available sugarcane bagasse promotes the valorization of agricultural waste, supporting cost-effectiveness and the circular economy principle.

The adsorption performance of the prepared Cs-Act SB adsorbent to ionic dyes was evaluated using anionic ARS as a model dye. The moisture content, ash content, and pH_{PZC} of the adsorbent were determined. Furthermore, the characterization of Cs-Act SB adsorbent was investigated using FTIR (Fourier-Transform Infrared Spectroscopy), SEM-EDX (Scanning Electron Microscopy-Energy Dispersive X-ray), and thermal analysis (Thermogravimetric Analysis). UV-Vis spectroscopy was used to examine the effect of various pH levels on the prepared CsAct-SB adsorbent's ability to remove the ARS dye.

2. Experimental

2.1. Materials

Chitosan (75-85% deacetylation) and acetic acid (CH_3COOH) were all analytical reagent grades and purchased from Sigma-Aldrich. Hydrochloric acid (HCl) (purity 37%), sodium hydroxide (NaOH), ethanol, nitric acid, and sodium bicarbonate were purchased from Merck. Alizarin Red S ($C_{14}H_8O_7S$) dye was used in this work. Table 1 presents the chemical structure and characteristics of the dye. A suitable quantity of the dye was dissolved to produce a stock solution with an initial concentration of 1000 mg L^{-1}.

2.2. Preparation of Sugarcane Bagasse Biochar (SB)

The preparation of SB, Act-SB, and Cs-Act SB was performed according to previously reported in the literature, with some modifications [26]. The sugarcane bagasse was collected from Colomadu District, Central Java, Indonesia. After being properly cleaned with deionized water and cut into small pieces, the material was dried at 105°C for 24 hours in a laboratory oven. The dried sugarcane bagasse was washed with 0.5% HCl to eliminate impurities and dried overnight at 110°C. Thereafter, it was carbonized for 2 hours at 600°C in a furnace to produce the sugarcane bagasse biochar (SB).

Table 1. Characteristic of ARS dye

Characteristic	
Name	Alizarin Red S
Chemical Structure	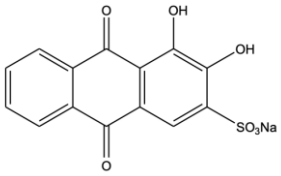
Synonym	3,4-dihydroxy-9,10-dioxo-2-anthracenesulfonic acid sodium salt
Formula	$C_{14}H_7NaO_7S$
Type dye	Anthraquinone
Molar mass (g.mol^{-1})	342.26
Color Index Number	58005
Color	Yellow below pH 3.7, yellow to purple between 3.7 and 5.0, and red at higher pH 5.0
Solubility in water	1 mg mL^{-1} (20°C)
λ_{max}	Acidic 434, neutral 423, basic 539 [27]

2.3. Preparation of Activated Carbon Derived from Sugarcane Bagasse (Act-SB)

The SB was immersed in a 2 M NaOH solution. The resulting sample was then dehydrated in an oven at 110°C and activated in a muffle furnace at 750°C for approximately 2 hours to produce activated carbon (Act-SB). The obtained Act-SB was rinsed with deionized water to remove any of the remaining contaminants until the pH of the filtrate reached 7-8. The Act-SB adsorbent was dried overnight in an oven at 120°C. The dried particles were pulverized and sieved. Particles between 250 and 300 µm were selected for chitosan (Cs) impregnation to preserve the structural stability of the adsorbent and maintain sufficient surface reactivity for an effective Cs modification. Similar particle-size selection has been reported in chitosan-based dye adsorption [28].

2.4. Preparation of Chitosan-Impregnated Activated Carbon Derived from Sugarcane Bagasse (Cs-Act SB)

The Cs-Act SB was prepared by dissolving 2 g of chitosan flakes in 100 mL of 2% v/v acetic acid solution while stirring constantly for 6 hours at 45°C. Following the complete dissolution of the chitosan, 2 g of Act-SB was added to the mixture and vigorously stirred for 6 hours at 45°C to produce Cs-Act SB. It was then filtered and washed thoroughly with distilled water until the pH was neutral. The prepared adsorbent was put in a desiccator for future use after being oven-dried overnight at 110°C. The illustration of preparation is shown in Figure 1.

2.5. Ash Content and Moisture Content Studies of Act-SB and Cs-Act SB

Approximately 0.5 g of prepared adsorbent was heated in a muffle furnace at 700°C for 6 hours, and then the final weight was measured. Furthermore, the moisture content was determined by heating 0.05 g of the prepared adsorbent in an oven at 110°C overnight. It was then allowed to cool to room temperature in a desiccator before being weighed. The dry weight of ash content and the moisture content of Cs-Act SB were calculated using Equation (1) and Equations (2) to (5), respectively.

$$Ash\ content\ (\%) = \frac{weight\ (ash+crucible) - weight\ (crucible)}{dry\ weight\ of\ the\ sample} \times 100 \quad (1)$$

$$Moisture\ content\ (\%) = \frac{loss\ in\ moisture\ (g)}{initial\ weight\ of\ the\ sample\ (g)} \times 100 \quad (2)$$

$$loss\ in\ moisture = initial\ weight\ (g) - final\ weight\ (g) \quad (3)$$

$$initial\ weight = wet\ or\ original\ weight\ of\ sample\ before\ drying \quad (4)$$

$$final\ weight = weight\ of\ sample\ after\ drying \quad (5)$$

2.6. Characterization of Act-SB and Cs-Act SB

A Hanna Instruments HI 2211 benchtop pH meter was used to test the pH of the buffer solutions and Alizarin Red S dye. The functional groups of the adsorbent were characterized using FTIR (Fourier Transform Infrared) spectroscopy (Prestige-21, Shimadzu). A SEM-EDX (FEI-Quanta 250) was used to investigate the surface morphology and chemical composition of the adsorbent. UV-Visible spectrophotometer (Shimadzu UV-Vis 1780) to determine the concentration of dye.

2.7. Determination of pH_{PZC}

Approximately 0.01 g of the Cs-Act SB was added to 15 mL of pH-adjusted NaCl (0.01 M) solution, which ranged from 2 to 12, and the mixtures were allowed to shake at the equilibrated shaker for 48 hours at ambient temperature. The pH of NaCl was adjusted using 0.1 M of HCl and 0.1 M of NaOH. The final pH was obtained after being shaken, and it was plotted against the initial pH (pH_i) using the formula $\Delta pH = pH_{initial} - pH_{final}$. The pH_{PZC} value is the cross point where the curve ΔpH versus pH_i crosses the line $\Delta pH = 0$.

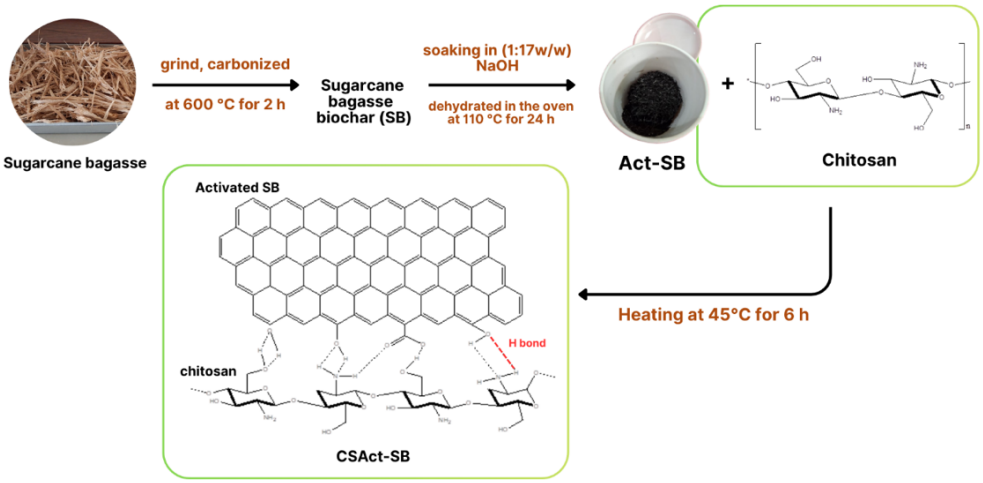

Figure 1. The schematic representation of the preparation of Cs-Act SB

2.8. Batch Adsorption Study

To investigate the effect of pH on the adsorption of ARS on Cs-Act SB, 0.05 g of adsorbent as the initial adsorbent dosage was added to 25 mL of 150 mg L^{-1} of dye solution, and pH was measured from 2 to 10 by adding 0.1 M NaOH and/or 0.1 M HCl for 60 minutes. All adsorption experiments were conducted at a constant agitation speed of 160 rpm. Meanwhile, for adsorbent dosage studies on ARS dye adsorption, the experiment was performed at various adsorbent dosage conditions (0.01-0.08 g) at an optimum pH of 2, with 25 mL of a 150 mg L^{-1} dye solution, and stirred for 60 minutes at a stirring speed of 150 rpm. The suspension was then centrifuged, and the supernatant was analyzed by UV-visible spectrophotometry. The absorbance of ARS was measured at 500 nm, which corresponds to the maximum absorption wavelength (λ_{max}) of ARS in the pH range used in this study, as confirmed by preliminary UV-Vis scans.

The amount of ARS in the samples was measured based on the standard curve. Five standard solutions, covering an ARS concentration range of 1–8 mg L^{-1}, were used for all calibrations to generate a standard curve. The removal efficiency (R, %) of ARS was determined according to Equation (6).

$$R\ (\%) = \frac{(C_0 - C_e)}{C_0} \times 100 \quad (6)$$

To calculate ARS concentration in the solution after each experiment, the adsorption capacity (q_e) was determined using Equation (7).

$$q_e = (C_0 - C_e) \times \frac{V}{m} \quad (7)$$

Where, C_0 (mg L^{-1}) and C_e (mg L^{-1}) are the initial and equilibrium ARS dye concentrations, respectively, while m (g) and V (L) are the weight of the adsorbent and the volume of aqueous solution, respectively.

2.9. Adsorption Kinetics

A total of 0.02 g of Cs-Act SB was added to 25 mL of 150 mg L^{-1} of ARS dye solution, and the adsorption process was conducted over varying contact times of 0, 20, 40, 60, 100, 120, 160, 200, 240, 280, 320, 360 minutes at a pH of 2. The data collected from these experiments were utilized to analyse the adsorption kinetics by fitting the results to various kinetic models, including pseudo-first-order (Equation 8) and pseudo-second-order (Equation 9) models.

$$\ln(q_e - q_t) = \ln q_e - k_1 t \quad (8)$$

$$\frac{t}{q_t} = \frac{1}{k_2 q_e^2} + \frac{1}{q_e} t \quad (9)$$

Where, C_A and C_0 are the concentrations at time t and initial time (mg L^{-1}), respectively. k is the rate constant, t is the contact time (min), q_e and q_t are the adsorbed amounts at equilibrium and at time t (mg g^{-1}), respectively.

2.10. Adsorption Isotherm

A total of 0.02 g of Cs-Act SB was added to 25 mL of ARS dye solution, and the adsorption process was conducted over varying concentrations of 40, 60, 80, 100, 120, 140, 160, 200, 250, and 300 mg L^{-1} at a pH of 2. The suspensions were agitated at the optimum contact time using a mechanical shaker. Afterward, the mixtures were filtered, and the filtrates were analyzed using a UV-Vis spectrophotometer. The data were then fitted to the Langmuir (Equation 10) and the Freundlich (Equation 11) isotherm models.

$$\frac{C_e}{Q_e} = \frac{1}{Q_m} C_e + \frac{1}{K_L Q_m} \quad (10)$$

$$\ln Q_e = ln\ K_F + \frac{1}{n} \ln C_e \quad (11)$$

Where, K_L (L mg^{-1}) and K_F ((mg g^{-1}) (L $mg^{-1})^{1/n}$) are the Langmuir and the Freundlich isotherm constants related to adsorption strength and capacity, respectively, $1/n$ is the heterogeneity factor of the Freundlich model, Q_e (mg g^{-1}) is the adsorption capacity of dye molecules at equilibrium, Q_m is the maximum adsorption capacity, and C_e (mg L^{-1}) is the concentration of the dye solution at adsorption equilibrium. Furthermore, the adsorption energies were calculated using the Gibbs energy ($\Delta G°$) (Equation 12).

$$\Delta G^{\circ} = -RT \ln(K) \quad (12)$$

Where, R is the thermodynamic gas constant (8.314 J $mol^{-1}K^{-1}$) and T (K) is the adsorption temperature. In the Langmuir equation, $K = b$, where b is the theoretical adsorption coefficient of Langmuir.

3. Results and Discussion

3.1. Ash Content and Moisture Content of Act-SB and Cs-Act SB

Cs-Act SB was synthesized using a two-step co-precipitation technique. The Act-SB was produced in the first stage by synthesizing sugarcane bagasse biochar and activating it with NaOH solution. The Cs-Act SB was produced in the second stage by impregnating Act-SB with chitosan solution. Both of Act-SB and Cs-Act SB are black in color.

As illustrated in Table 2, the moisture content of Cs-Act SB adsorbent was 4%, indicating a high surface area and a large number of active sites. It also demonstrated the existence of a hydrophilic functional group on the hydrophobic adsorbent surface. Furthermore, the ash content was low, around 3.4%. This can be ascertained and verified by elemental analysis, which validates the high carbon content compared to other elements.

3.2. Adsorbent Characterization

3.2.1. FTIR analysis

The FTIR spectra for SB, Act-SB, and Cs-Act SB are presented in Figure 2. The spectra show that all samples have a broad peak between 3430 cm^{-1} and 3401 cm^{-1}, which is attributed to the O–H or N–H stretching region [29]. In Act-SB, a peak at 3402 cm^{-1} corresponds to the O– H stretching vibration. Meanwhile, after chitosan modification, the basic characteristic peaks of the chitosan were shown for Cs-Act SB at 3440 cm^{-1} due to the stretching vibration of hydroxyl and amino functional group (O–H stretching and N–H stretching, overlapped) [30]. These peaks confirm the success of the synthesis of the Cs-Act SB. Furthermore, peaks at 3061 cm^{-1} and 2956 cm^{-1} correspond to the C–H stretching vibration. The peak around 1577 cm^{-1} exhibits the presence of C–N stretching and N–H bending vibrations.

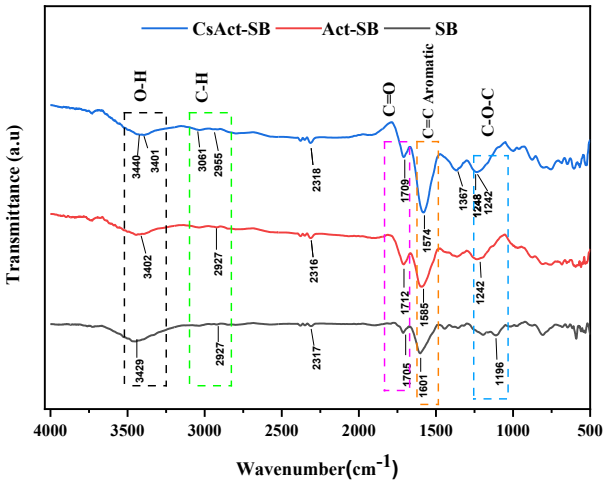

Figure 2. The FTIR spectra of Cs-Act SB, Act-SB, and SB

Table 2. Ash and moisture content of the adsorbent

Adsorbent	Ash content (%)	Moisture content (%)
Act-SB	1.6	10
CsAct-SB	3.4	4

Moreover, a peak corresponding to C=O stretching is observed in the range of 1705 cm^{-1} to 1710 cm^{-1}, suggesting the carboxyl groups are present in all samples [31]. The C=O stretching and C=C vibrations of aromatic structures in lignin are linked to the bands present in SB and Act-SB between 1711 and 1586 cm^{-1} [32]. The peak at 1242 cm^{-1} to 1197 cm^{-1}, which corresponds to C–O–C vibrations in cellulose and hemicellulose, is observed [33]. In conclusion, the efficient synthesis of the Cs-Act SB adsorbent has been further confirmed by the observation of functional groups that contribute to the effective adsorption process, including hydroxyl, amino, carboxyl, and aliphatic groups.

3.2.2. SEM-EDX analysis

Analysis of surface morphology and elemental determination was performed using a Scanning Electron Microscope coupled with an Energy-Dispersive Spectrometer. The surface morphological properties and EDX of the SB biochar, Act-SB, and Cs-Act SB are represented in Figures 3 and 4.

A noticeable difference can be observed between the activated carbon before and after impregnation with chitosan. Before impregnation, the material is more regular in nature with a smooth texture. After chitosan impregnation, the surface of Cs-Act SB has an irregular and heterogeneous surface. This indicates that an interaction between Act-SB and chitosan had occurred. Moreover, the porous and folded surface of the adsorbent increases its surface area and, consequently, its adsorption capacity.

The elemental composition of Cs-Act SB was examined using the EDX. Based on the EDX spectra of SB, Act-SB, and Cs-Act SB, all materials contain carbon and oxygen as constituent elements, along with a slight impurity of Ca in Act-SB and Cs-Act SB. Before chitosan impregnation, the carbon and oxygen content in Act-SB were 80.71% and 19.04%, respectively. These results were similar to the previous study, that the percentage of carbon in sugarcane bagasse after the activation process was 80.13% [34]. After impregnation, the carbon and oxygen content were found to be slightly higher than those of Act-SB.

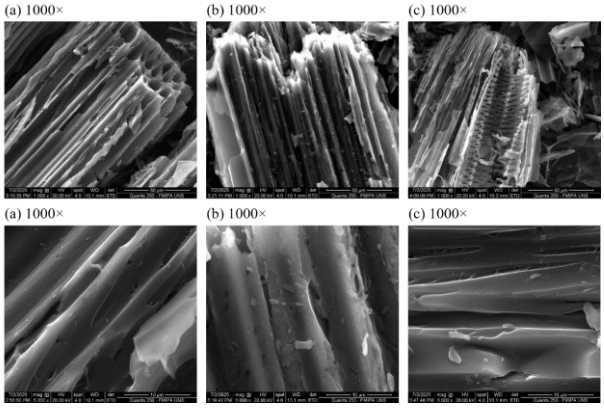

Figure 3. Morphology of (a) SB, (b) Act-SB, (c) Cs-Act SB at 1000× and 5000× magnifications

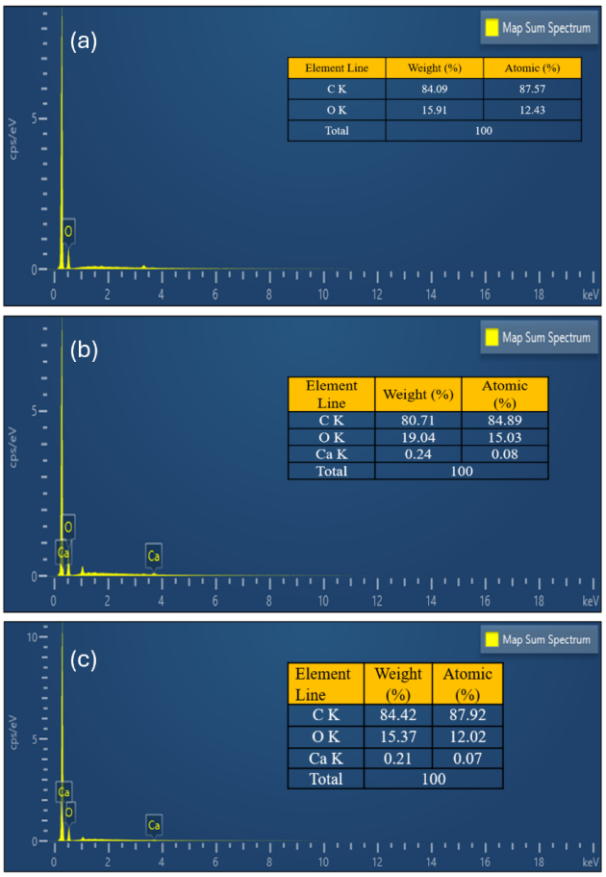

Figure 4. EDX of (a) SB, (b) Act-SB, and (c) Cs-Act SB

3.2.3. Thermogravimetric Analysis

Thermogravimetric analysis (TGA) was employed to investigate the thermal behaviour of the prepared Cs-Act SB. The Cs-Act SB is thermally evaluated in a 25-700°C temperature range to determine the thermal stability against temperature. The weight loss is recorded when the temperature is raised to 700°C.

From Figure 5, Cs-Act SB exhibits two decomposition steps. The first stage, characterized by a weight loss of 11.99%, is observed when the temperature is increased from 30°C to 120°C, attributed to the evaporation of water from the adsorbent surface and its moisture content [35]. The second loss occurred in the range of 325-400°C. This is probably caused by thermal degradation of volatile components in the material, including dehydration of saccharide rings, polymerization, and decomposition of polymer units [36]. Moreover, the complete degradation above 500°C indicates the stability of this adsorbent against high temperatures.

3.3. Determination of the Point of Zero Charge (pH_{PZC})

The pH_{PZC} is a crucial factor in adsorption processes. The pH_{PZC} is the pH at which the adsorbent surface has an equal quantity of positive and negative charges, resulting in a net zero charge, or the state at which the density of electrical charge on a surface is equal to zero. Figure 6 shows that the pH_{PZC} of the Cs-Act SB was 4.58, indicating that there was no net charge on the surface of the adsorbent at this pH.

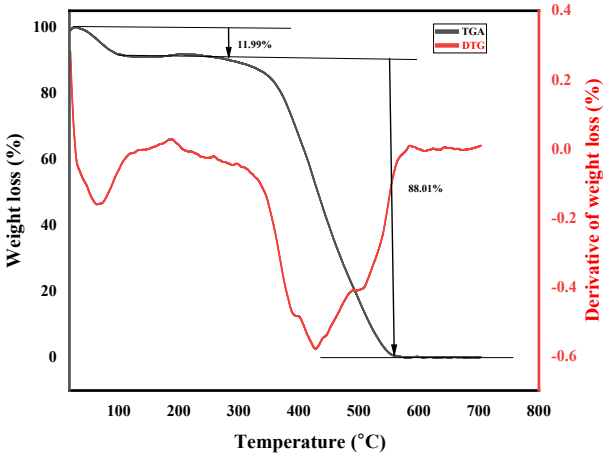

Figure 5. The thermogravimetric curves for Cs-Act SB

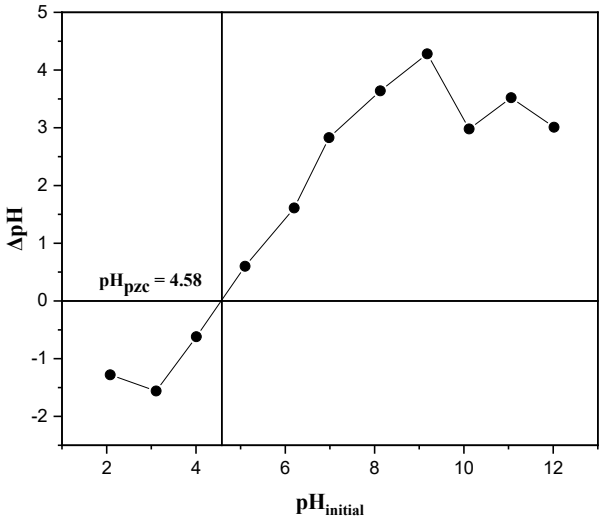

Figure 6. The pH_{PZC} for Cs-Act SB

A pH below pH_{PZC} (lower than 4.58) indicates that the amine group in chitosan has been protonated. By adding a proton to the amine groups, the surface of the chitosan becomes positively charged [27]. As a result, in acidic conditions (pH was lower than pH_{PZC}), the amine groups were likely to be positively charged due to protonation, affecting the surface charge properties of the Cs-Act SB.

3.4. The Effect of pH on ARS Dye Adsorption

The pH of the aqueous solution is a significant factor influencing the adsorption characteristics of both the adsorbent and the adsorbate. The pH influences the surface polarity of the Cs-Act SB adsorbent, ionic mobility, and chemical properties of the ARS dye solution. Electrostatic interaction between adsorbate and adsorbents can occur because both adsorbent and adsorbate may contain functional groups that can be protonated or deprotonated to produce different surface charges in solution at various pH values [37]. The effect of pH on the removal of ARS using the Cs-Act SB is presented in Figure 7.

The pH_{PZC} of the Cs-Act SB was found to be 4.58, indicating that the adsorbent surface is positively charged below this pH and negatively charged above it. This effect is attributed to the functional groups present in the adsorbent. At low pH, the amine groups ($-NH_2$) in

chitosan become protonated ($-NH_3^+$), making the surface cationic. As the pH rises, these groups deprotonate, leaving a negative charge on the surface [38]. Consequently, when the solution pH exceeds the pH_{PZC}, the negatively charged surface favors adsorption of cationic dyes; when the pH is lower, the adsorbent surface becomes positively charged, which subsequently adsorbs the anionic dye [39]. This leads to a greater degree of electrostatic interaction between the adsorbent surface and ARS dye molecules. This correlation accounts for the enhancement in adsorption capacity at low pH (particularly at pH 2, where the surface becomes the most protonated).

The sulfonate groups ($-SO_3^-$) in ARS are negatively charged in aqueous solution, making it an anionic dye. In general, anionic dye adsorption is greatly enhanced with pH < pH_{PZC}. Under these conditions, the surface is positively charged and could favor the electrostatic attraction of the ARS anionic dyes used in the present work [40, 41]. Furthermore, ARS is an anionic dye having sulfonic acid and phenolic groups that deprotonate in aqueous solution when the pH shifts. At about 5.5 pKa, the phenolic group in ARS dye dissociates, changing the charge distribution. ARS is largely protonated or slightly deprotonated at low pH (pH < 5.5) and completely deprotonated and negatively charged at higher pH [42].

According to Figure 7, the removal of ARS decreases from 71.54 mg g^{-1} at pH = 2 to 66.91 mg g^{-1} at pH = 3 for Cs-Act SB and decreases from 66.02 mg g^{-1} at pH = 4 to 64.77 mg g^{-1} at pH = 12. Thus, as the pH of the solution increases, the adsorption capacity decreases. Due to electrostatic repulsion between negatively charged sites on the adsorbent and anionic dyes, as well as the sequential deprotonation of positively charged groups on the adsorbent, a decrease in adsorption occurred as the pH of the ARS dye increased. Additionally, the OH^- and dye anions competed for the positively charged adsorption sites, which led to a decrease in the removal of ARS dye under alkaline pH conditions [26]. Based on these findings, pH 2 was identified as the optimum pH for ARS dye adsorption onto adsorbents and was used in all subsequent experiments.

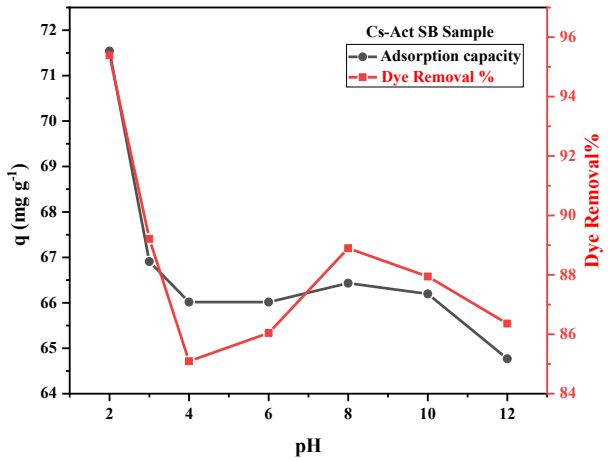

Figure 7. Effect of pH on the adsorption capacity of ARS dye onto Cs-Act SB (Conditions: 0.05 g adsorbent, 25 mL of 150 mg L^{-1} ARS dye, stirring time of 60 minutes at room temperature, stirring speed of 150 rpm)

3.5. Effect of Adsorbent Dosage on ARS Dye Adsorption

The adsorbent dosage has a significant impact on the distribution and arrangement of adsorbate molecules on the adsorbent surface. Different adsorbent dosages were examined, ranging from 0.01 to 0.08 g at a pH of 2, while keeping the initial concentration of dye constant at 150 mg L^{-1}, stirring speed (150 rpm), and contact time (60 minutes). The ARS adsorption was measured using a UV-visible spectrophotometer.

According to Figure 8, the percentage of dye removal increases with higher adsorbent dosage, reaching 99.9% for Cs-Act SB at 0.02 g and 98.5% for Act-SB at 0.04 g in a 150 mg L^{-1} ARS dye solution. Furthermore, since the majority of the accessible binding sites are already occupied, the saturation of active sites on the adsorbent surface limits further adsorption, resulting in a decline in adsorption efficiency beyond the optimum adsorbent dosage. Similar adsorption behaviour has been reported for ARS dye adsorption, where the saturation of active sites prevents additional increases from appreciably improving removal efficiency [38]. Meanwhile, an inverse relationship was observed between the adsorption capacity and the dosage of the adsorbent. This finding was possible due to the availability of a large number of dye molecules, which is sufficient to saturate the adsorption sites with minimum competition.

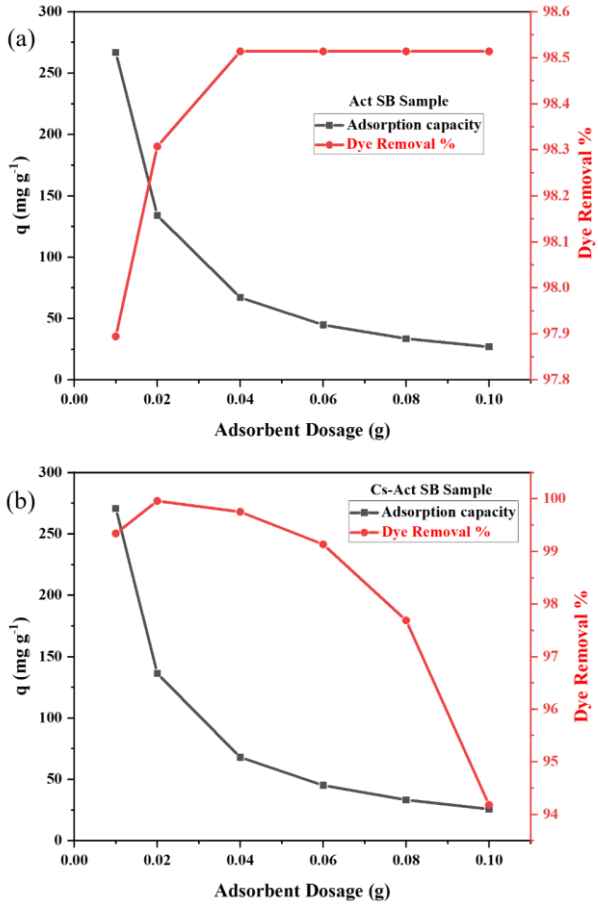

Figure 8. Effect of adsorbent dosage on adsorption capacity of ARS dye onto (a) Act-SB and (b) Cs-Act SB (Conditions: pH 2.0, 25 mL of 150 mg L^{-1} ARS dye, stirring time of 60 minutes at room temperature, stirring speed of 150 rpm)

According to Figure 8, the amount of adsorbate adsorbed gradually decreased from 0.04 to 0.1 g. This is because more active sites were introduced into the adsorption system while the adsorbate concentration remained constant. In this instance, the splitting of the available adsorbate concentration gradient reduces the driving force on the active sites. Additionally, there is a chance that particles will aggregate, which will eventually decrease the surface area of the adsorbents at higher dosages [43].

3.6. Adsorption Kinetics

The adsorption kinetics of ARS on Cs-Act SB were examined in aqueous solution. The adsorption process reached equilibrium values (corresponding to the plateau, as shown in Figure 9(a) in 120 minutes. Under the conditions of pH = 2, initial ARS dye concentration of 150 ppm, and adsorbent dosage of 0.02 mg, the adsorption capacity (q_e) of ARS on Cs-Act SB was 116.77 mg g^{-1}.

The experimental data were fitted to pseudo-first-order and pseudo-second-order kinetic models, with the resulting parameters shown in Table 3. Based on the data, fitting the experimental data using the pseudo-first-order model yielded low correlation coefficients, thus demonstrating the inadequacy of this model in describing ARS dye adsorption on Cs-Act SB and Act-SB as well. Meanwhile, the pseudo-second-order model yielded a very good fit, as evidenced by the high correlation coefficient (R > 0.99).

Moreover, the pseudo-second-order kinetic model was considered, which shows a linear relationship between the adsorption rate and reactant concentration, including that of the adsorbent and adsorbate. The adsorption capacity (q_e) calculated from the pseudo-second order is very similar to the experimentally observed values (117.65 mg g^{-1} for Cs-Act SB and 21.83 mg g^{-1} for Act-SB). The use of the pseudo-second-order kinetic model meant that the chemical interactions of the ARS dye molecule with the adsorbent surface involved electron transfers. To obtain the equilibrium concentration, the first phase consisted of quick chemisorption of the dye molecules on the adsorbent, followed by the second slow phase of physisorption [44].

Table 3. Parameters of the kinetics model for ARS dye adsorption onto Cs-Act SB and Act-SB

Kinetics model	Cs-Act SB	Act-SB
Pseudo-first order		
q_e *exp* (mg g^{-1})	116.77	22.03
k_1 (min^{-1})	0.0067	0.0086
q_e *cal* (mg g^{-1})	4.658	7.549
R^2	0.302	0.724
Pseudo-second order		
q_e *exp* (mg g^{-1})	116.77	22.03
k_2 (g mg^{-1} min^{-1})	0.011	0.006
q_e *cal* (mg g^{-1})	117.65	21.83
R^2	1	0.997
h (mg g^{-1} min^{-1})	149.25	2.67

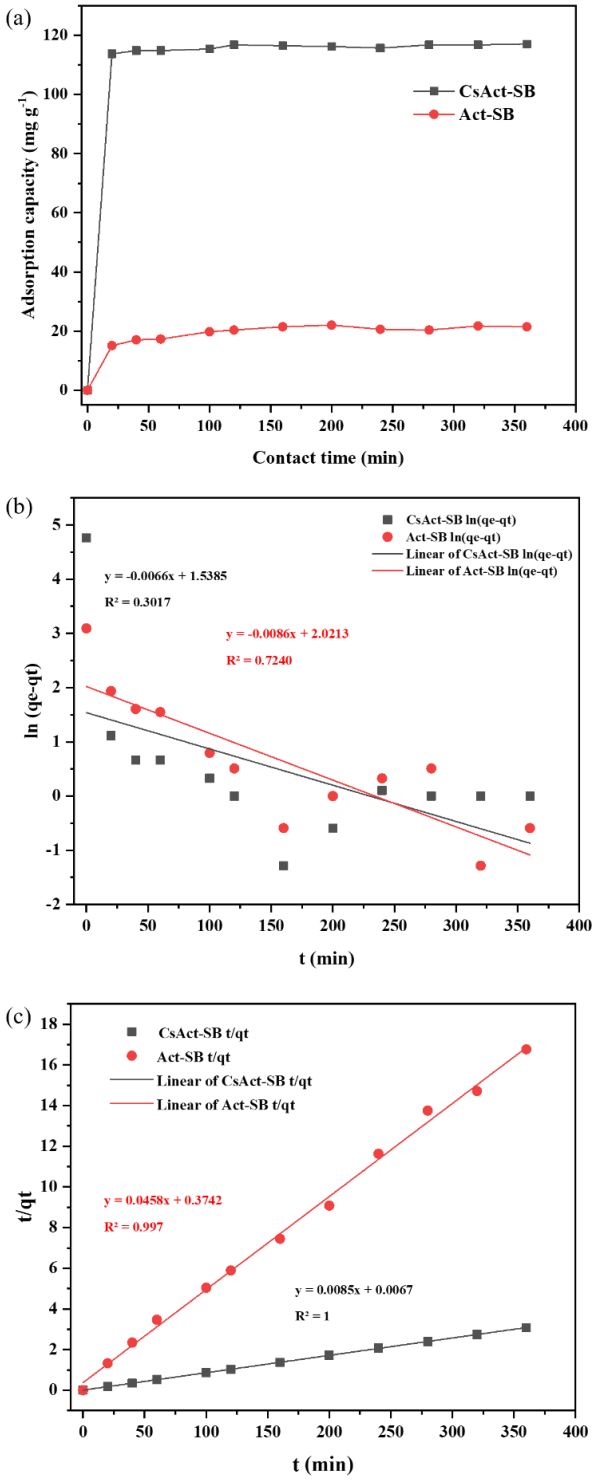

Figure 9. (a) Effect of contact time on the adsorption of alizarin red S dye on Cs-Act SB and Act-SB. The data were fit using kinetics models; (b) Pseudo-first order model; (c) Pseudo-second order kinetic models (Conditions: pH 2.0, 25 mL of 150 mg L^{-1} ARS dye, adsorbent dosage of 0.02 g, stirring speed of 150 rpm at room temperature)

One notable study by Rashda *et al.* [45] demonstrated that the adsorption of alizarin red S and 2,4-dichlorphenoxyacetic acid from wastewater onto chitosan and iron oxide-coated peanut husk-activated carbon (CS/Fe_3O_4-NPs@PHAC) followed the pseudo-second-order model. Moreover, a similar result reported that the pseudo-second-order kinetic model was

effectively adequate for describing the sorption of alizarin red S dye on biochar-based adsorbents (Fe_2O_3@biochar and Fe_2O_3@biochar-kaolinite clay composite) [46].

Furthermore, Moheb *et al.* [47] focused on the adsorption of alizarin red S and methylene blue onto a highly porous activated carbon derived from a papaya plant. The pseudo-second-order kinetic model was more suitable for describing the dynamic behavior of methylene blue and alizarin red S adsorption compared to the pseudo-first-order model, indicating a chemisorption process involving electron sharing or transfer between the adsorbent and adsorbate.

3.7. Isotherm Adsorption

The adsorption isotherms of ARS dye were conducted at various initial concentrations (10-160 mg L^{-1}) to analyze how the adsorption capacity is affected by the initial concentration of the dye. The other adsorption conditions were kept constant at an optimum pH of 2, an adsorbent dosage of 0.02 g, 25 mL of ARS dye, and contact times of 120 and 200 minutes for Cs-Act SB and Act-SB, respectively. To comprehend the adsorption mechanism of ARS dye on Cs-Act SB and Act-SB, the Langmuir and the Freundlich isotherm models were then used to assess the results.

The effect of the initial concentration of ARS dye on the amount of ARS dye on Cs-Act SB and Act-SB is shown in Figure 10 (a). It has been observed that the initial concentration of metal ions affects the adsorption capacity of adsorbed ARS dye on the adsorbents. Generally, the amount of ARS dye adsorbed increases from 40 to 160 ppm, indicating that the adsorbate has not yet completely occupied all the accessible active sites on the adsorbent surface. Then, further increasing the initial concentration of ARS dye has no noticeable impact on the adsorption capacity of either Cs-Act SB or Act-SB. This result indicates that the equilibrium has been reached between ARS dye and the adsorbents; thus, the ARS dye can no longer occupy the active sites of the adsorbents.

The experimental data were analyzed using a fitting procedure based on two linearized isotherm models, namely the Langmuir and the Freundlich models. The adsorption isotherms of ARS on Cs-Act SB and Act-SB are shown in Figure 10. The determined values for the isotherm parameters are given in Table 4. Based on the correlation coefficient (R^2) values, the experimental data fit the Langmuir isotherm model better than the Freundlich isotherm model. This implied that the adsorption layer of the ARS dye onto the Cs-Act SB and Act-SB surface occurred in a homogeneous monolayer. The determined Langmuir maximum adsorption capacity of Cs-Act SB and Act-SB for the ARS dye adsorption were 78.13 mg g^{-1} and 30.03 mg g^{-1}, respectively. These results indicate that Cs-Act SB exhibited a higher affinity toward ARS dye due to the synergistic effect of chitosan modification, which provides more active functional sites.

Based on Table 4, the adsorption energies were 36.05 kJ mol^{-1} for Cs-Act SB and 27.25 kJ mol^{-1} for Act SB. The energy of physical adsorption is generally below 4.18 kJ mol^{-1}, whereas the energy of chemical adsorption is typically above 20.92 kJ mol^{-1} [48]. The results of this study indicate that the adsorption of ARS dye on the Cs-Act SB adsorbent was a chemisorption process rather than physisorption.

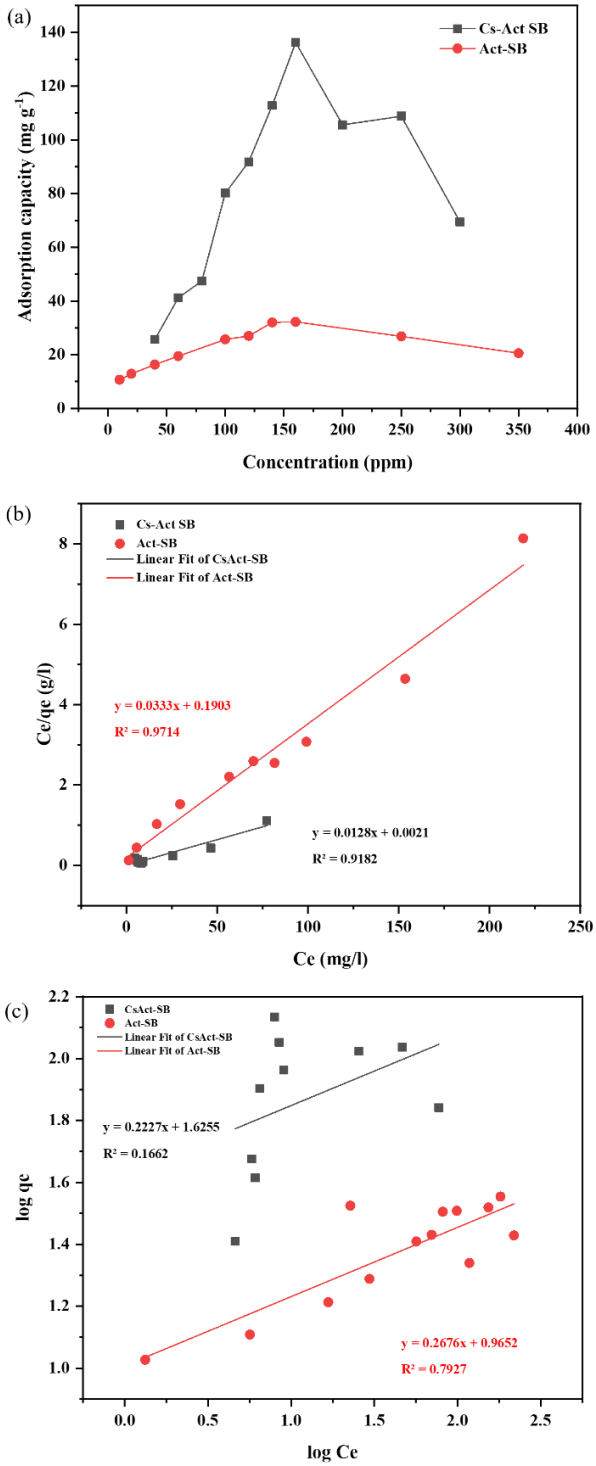

Figure 10. (a) Effect of concentration on the adsorption of alizarin red S dye on Cs-Act SB and Act-SB. Adsorption data were fitted using isotherm models: (b) Langmuir; (c) Freundlich (Conditions: pH 2.0, adsorbent dosage of 0.02 g, contact time of 120 and 200 minutes for Cs-Act SB and Act-SB, respectively, and a stirring speed of 150 rpm at room temperature)

Table 4. Langmuir isothermal adsorption parameters on Cs-Act SB and Act-SB

Adsorbent	Langmuir isothermal adsorption parameters			
	Adsorption capacity ($q_{e\ max}$) (mg g^{-1})	Equilibrium constants (K_L) (mol^{-1} L)	Adsorption energy (kJ mol^{-1})	Plot linearity (R^2)
Cs-Act SB	78.13	2.09 × 106	36.05	0.9182
Act-SB	30.03	5.99 × 104	27.25	0.9714

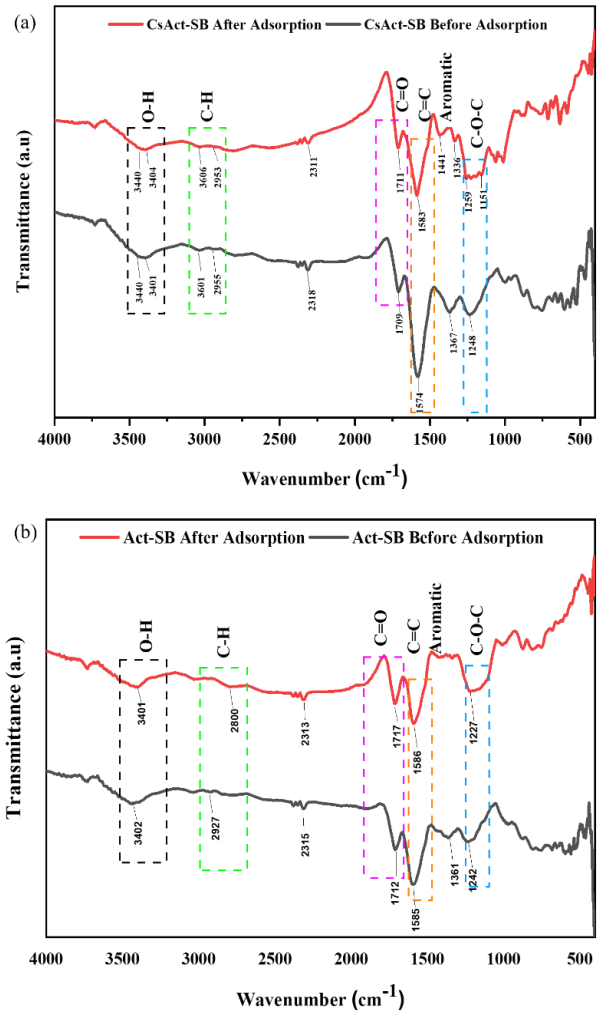

Figure 11. FTIR spectra of the adsorbents before and after adsorption (a) Cs-Act SB and (b) Act-SB

Moreover, to assess the performance, the maximum adsorption capacity of Cs-Act SB was compared with that of other adsorbents for ARS dye removal, as presented in Table 5. Although some adsorbents, such as $NiFe_2O_4$/polyaniline (PANI) magnetic composite and Zr/diethylenetriamine functionalized wheat straw, show higher adsorption capacities, the obtained value for Cs-Act SB (78.13 mg g^{-1}) remains practically significant. Its performance exceeds that of several other biomass-based materials, such as immobilized *Canna indica* biomass (21.69 mg g^{-1}) and banana fiber carbon (65.07 mg g^{-1}).

The potential scalability and cost-effectiveness of Cs-Act SB were supported by its simple and mild preparation. Moreover, sugarcane bagasse, a locally accessible agricultural waste, provides an environmentally friendly, affordable, and renewable resource for wastewater treatment applications.

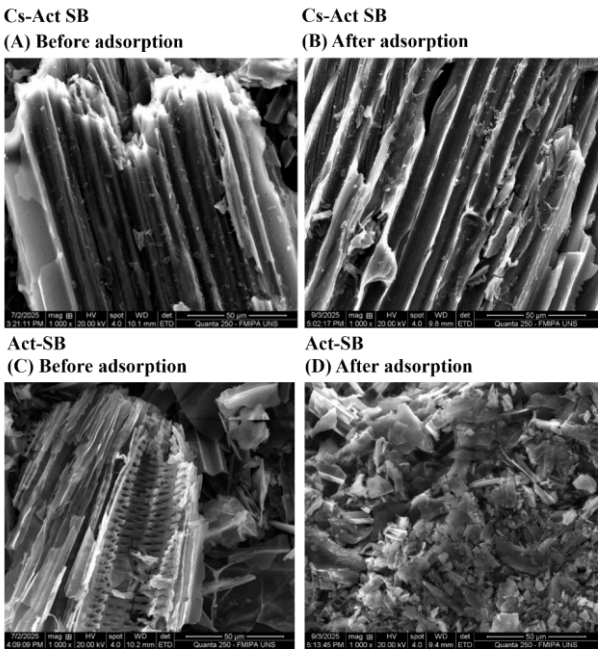

Figure 12. SEM images of Cs-Act SB (1000×) before adsorption (A), after adsorption (B), and Act-SB (1000×) before adsorption (C), after adsorption (D)

3.8. After Adsorption

The FTIR spectra of the CsAct-SB and Act-SB before and after adsorption of ARS dye were compared in Figure 11. This reveals changes in its functional groups, including peak shift, new peak appearances, and changes in peak intensity, indicating interactions between ARS and the adsorbent. From the spectra, the increment of the peak situated at 1574 cm^{-1}, which demonstrates the presence of C=C in CsAct-SB, shifted toward 1583 cm^{-1}. Before adsorption, Cs-Act SB exhibits peaks at 3440 cm^{-1} and 3401 cm^{-1} due to the stretching vibration of hydroxyl and amino functional group (O–H stretching and N–H stretching, overlapped). Meanwhile, the peak shifted slightly to 3440 cm^{-1} and 3404 cm^{-1} after adsorption.

Moreover, several new peaks appeared, indicating the interaction between the ARS and the adsorbent. The peak at 1441 cm^{-1} is due to symmetrical C-H bending. In addition, the absorption band at 1336 cm^{-1} is due to the aromatic stretching, and 1151 cm^{-1} may be due to the stretching of S=O in SO_3.

Furthermore, based on the morphology shown in Figure 12, a noticeable difference is observed between the samples before and after impregnation with activated carbon and chitosan. Previously, the material exhibited open pores and a rough surface. Meanwhile, the adsorbent material became partially closed and denser after being impregnated with chitosan.

Table 5. The comparison of the maximum adsorption capacity (q_{max}) for ARS dye removal with other adsorbents

Adsorbent	Adsorption capacity, q_{max} (mg g^{-1})	Reference
Magnetic activated carbon (MAC) nanocomposite	108.69	[37]
$NiFe_2O_4$/polyaniline (PANI) magnetic composite	186	[49]
Immobilized biomass of *Canna indica*	21.69	[50]
Zirconium and diethylenetriamine functionalized wheat straw	164	[51]
Sono-synthesized LDHs/g-C_3N_4 nanocomposite	48.08	[52]
The hollow tube-like banana fibre carbon (BFC)	65.07	[53]
Chitosan-impregnated sugarcane bagasse activated carbon (Cs- Act SB)	78.13	This study

4. Conclusion

A chitosan-impregnated activated carbon derived from sugarcane bagasse (Cs-Act SB) was successfully synthesized and thoroughly characterized. The prepared material was used to remove the ARS dye using batch experiments. The results indicated that the adsorption capacity was dependent on the pH, adsorbent dosage, contact time, and the concentration of ARS dye. The kinetic and isotherm studies revealed that the adsorption followed a pseudo-second-order and Langmuir model, with a maximum capacity of 78.13 mg g^{-1}, which is comparable to that of many reported adsorbents. Chitosan impregnation enhanced the adsorbent performance by approximately 2.6 times compared to unmodified activated carbon.

Acknowledgments

The authors acknowledge the financial support from RKAT Universitas Sebelas Maret (UNS), Surakarta, Indonesia, through the PKGR-UNS A Scheme Grant No. 371/UN27.22/PT.01.03/2025.

References

[1] S. Aravindhan, G. Bharath Kumar, M. Saravanan, A. Arumugam, Delonix regia biomass as an eco-friendly biosorbent for effective Alizarin Red S textile dye removal: Characterization, kinetics, and isotherm studies, *Bioresource Technology Reports*, 25, (2024), 101721 https://doi.org/10.1016/j.biteb.2023.101721

[2] Parya Ezati, Jong-Whan Rhim, Mehran Moradi, Hossein Tajik, Rahim Molaei, CMC and CNF-based alizarin incorporated reversible pH-responsive color indicator films, *Carbohydrate Polymers*, 246, (2020), 116614 https://doi.org/10.1016/j.carbpol.2020.116614

[3] M. H. Connolly, P. C. Yelick, High-throughput methods for visualizing the teleost skeleton: capturing autofluorescence of alizarin red, *Journal of Applied Ichthyology*, 26, 2, (2010), 274-277 https://doi.org/10.1111/j.1439-0426.2010.01419.x

[4] Jinfeng Zhou, Yuqian Sun, Chuanqiang Zhou, Xiaohuan Sun, Jie Han, Polyaniline/carbon hybrids: Synthesis and application for alizarin red S removal from water, *Colloids and Surfaces A: Physicochemical and Engineering Aspects*, 676, (2023), 132204 https://doi.org/10.1016/j.colsurfa.2023.132204

[5] Xiaohui Mao, Jiaqi Li, Yinghui Li, Tian Si, Jie Shang, Shengbao Cai, Xin Gao, Lincai Peng, Heng Zhang, The top-down construction of cornstalk-based columns as self-adaptive bio-adsorbents for selective dye adsorption from wastewater, *Separation and Purification Technology*, 359, (2025), 130493 https://doi.org/10.1016/j.seppur.2024.130493

[6] Asmaa Abuessawy, Amr Fouda, Adel A. H. Abdel-Rahman, Mohamed A. Hawata, Nora A. Hamad, A new Modified Heterocyclic-Magnetite Chitosan Nanocomposite for Efficient Alizarin Red Dye Removal: Adsorption Analysis and Antibacterial Activity, *Journal of Polymers and the Environment*, 32, 2, (2024), 826-841 https://doi.org/10.1007/s10924-023-03002-w

[7] George Joseph, Sunaja Devi Kalathiparambil Rajendra Pai, Arun Varghese, Dephan Pinheiro, Mothi Krishna Mohan, Sony J. Chundattu, Adsorptive capacity of PANI/Bi_2O_3 composite through isotherm and kinetics studies on alizarin red, *Journal of Molecular Structure*, 1308, (2024), 138095 https://doi.org/10.1016/j.molstruc.2024.138095

[8] Jisha Joseph, Raji Chorenjeth Radhakrishnan, Johnly Kannanaikkal Johnson, Steny Pereppadan Joy, Jency Thomas, Ion-exchange mediated removal of cationic dye-stuffs from water using ammonium phosphomolybdate, *Materials Chemistry and Physics*, 242, (2020), 122488 https://doi.org/10.1016/j.matchemphys.2019.122488

[9] Chensi Shen, Yuting Pan, Deli Wu, Yanbiao Liu, Chunyan Ma, Fang Li, Huijie Ma, Yaopeng Zhang, A crosslinking-induced precipitation process for the simultaneous removal of poly(vinyl alcohol) and reactive dye: The importance of covalent bond forming and magnesium coagulation, *Chemical Engineering Journal*, 374, (2019), 904-913 https://doi.org/10.1016/j.cej.2019.05.203

[10] Yushu Sui, Zhonghua Tang, Yixuan Liu, Xin Tong, Ning Chen, Dongru Chen, Qiuyu Miao, Yan Wang, Xiaorui Guo, Ning Cao, Jinhui Pang, Mixed dimensional assembly of biodegradable and antifouling wood-based covalent organic framework composite membranes for rapid and efficient dye/salt separation, *Journal of Hazardous Materials*, 480, (2024), 136012 https://doi.org/10.1016/j.jhazmat.2024.136012

[11] Zabihollah Yousefi, Ali Zafarzadeh, Reza Ali Mohammadpour, Ebrahim Zarei, Nezamaddin

Mengelizadeh, Abdolaziz Ghezel, Electrochemical removal of acid red 18 dye from synthetic wastewater using a three-dimensional electrochemical reactor, *Desalination and Water Treatment*, 165, (2019), 352-361 https://doi.org/10.5004/dwt.2019.24502

[12] Tayyaba Jamil, Role of advance oxidation processes (AOPs) in textile wastewater treatment: A critical review, *Desalination and Water Treatment*, 318, (2024), 100387 https://doi.org/10.1016/j.dwt.2024.100387

[13] M. M. Hassan, Z. N. Abudi, M. H. Al-Furaiji, Polysulfone Ultrafiltration Membranes Embedded with Silica Nanoparticles for Enhanced Dye Removal Performance, *Progress in Color, Colorants and Coatings*, 16, 2, (2023), 165-179 https://doi.org/10.30509/pccc.2022.167016.1185

[14] Amir Ikhlaq, Sidra Shabbir, Farhan Javed, Mosin Kazmi, Abdullah Yasir, Umair Yaqub Qazi, Mahrukh Zafar, Fei Qi, Catalytic ozonation combined electroflocculation for the removal of Reactive Black 5 in aqueous solution using $CuMn_2O_4$/RGO coated zeolites, *Desalination and Water Treatment*, 259, (2022), 221-229 https://doi.org/10.5004/dwt.2022.28435

[15] Giulia Rossella Delpiano, Davide Tocco, Luca Medda, Edmond Magner, Andrea Salis, Adsorption of Malachite Green and Alizarin Red S Dyes Using Fe-BTC Metal Organic Framework as Adsorbent, *International Journal of Molecular Sciences*, 22, 2, (2021), 788 https://doi.org/10.3390/ijms22020788

[16] Tahani saad Algarni, Amal M. Al-Mohaimeed, Water purification by adsorption of pigments or pollutants via metaloxide, *Journal of King Saud University – Science*, 34, 102339 https://doi.org/10.1016/j.jksus.2022.102339

[17] Seda Karayünlü Bozbaş, Deniz Bingöl, Investigation of adsorption potential of waste jewelry meerschaum powder for Cu(II) and cationic dye, *Scientific Reports*, 14, 1, (2024), 17193 https://doi.org/10.1038/s41598-024-66050-9

[18] Kuljit Kaur, Rajandeep Kaur, Harpreet Kaur, A systematic review of lignocellulosic biomass for remediation of environmental pollutants, *Applied Surface Science Advances*, 19, (2024), 100547 https://doi.org/10.1016/j.apsadv.2023.100547

[19] Hamad Hussain Shah, Muhammad Amin, Francesco Pepe, Erasmo Mancusi, Anaiz Gul Fareed, Overview of environmental and economic viability of activated carbons derived from waste biomass for adsorptive water treatment applications, *Environmental Science and Pollution Research*, 32, 32, (2025), 19084-19109 https://doi.org/10.1007/s11356-023-30540-6

[20] Urooj Kamran, Haq Nawaz Bhatti, Saima Noreen, Muhammad Asif Tahir, Soo-Jin Park, Chemically modified sugarcane bagasse-based biocomposites for efficient removal of acid red 1 dye: Kinetics, isotherms, thermodynamics, and desorption studies, *Chemosphere*, 291, (2022), 132796 https://doi.org/10.1016/j.chemosphere.2021.132796

[21] Pengcheng Luan, Jianming Liao, Li Chen, Yishan Kuang, Xi Zhang, Yuxiang Zhang, Yikui Zhu, Yonghong Dai, Lihuan Mo, Jun Li, Facile and sustainable modification for improving the adsorption ability of sugarcane bagasse towards cationic organic pollutants, *Biomass Conversion and Biorefinery*, 14, 3, (2024), 4055-4070 https://doi.org/10.1007/s13399-022-02551-9

[22] Alusani Manyatshe, Zamani E. D. Cele, Mohammed O. Balogun, Thabo T. I. Nkambule, Titus A. M. Msagati, Chitosan modified sugarcane bagasse biochar for the adsorption of inorganic phosphate ions from aqueous solution, *Journal of Environmental Chemical Engineering*, 10, 5, (2022), 108243 https://doi.org/10.1016/j.jece.2022.108243

[23] Aqsa Rukhsar, Zeenat Fatima Iqbal, Muhammad Shahzeb Khan, Syeda Alvia Zainab, Shahid Nawaz, Tak H. Kim, Ghulam Mustafa, Aldona Balčiūnaitė, Chitosan-Based Adsorbents and Catalysts for Removal of Toxic Pollutants from Water and Wastewater, *Topics in Catalysis*, 68, 9, (2025), 893-915 https://doi.org/10.1007/s11244-024-01979-9

[24] Estefânia V. R. Campos, Jhones L. Oliveira, Leonardo F. Fraceto, Poly(ethylene glycol) and Cyclodextrin-Grafted Chitosan: From Methodologies to Preparation and Potential Biotechnological Applications, *Frontiers in Chemistry*, Volume 5 - 2017, (2017), https://doi.org/10.3389/fchem.2017.00093

[25] Jianzhong Guo, Shunwei Chen, Li Liu, Bing Li, Ping Yang, Lijun Zhang, Yanlong Feng, Adsorption of dye from wastewater using chitosan–CTAB modified bentonites, *Journal of Colloid and Interface Science*, 382, 1, (2012), 61-66 https://doi.org/10.1016/j.jcis.2012.05.044

[26] Magda A. Akl, Asmaa A. Serage, Chitosan impregnated sugarcane bagasse biochar for removal of anionic dyes from wastewater, *Scientific Reports*, 14, 1, (2024), 27097 https://doi.org/10.1038/s41598-024-77708-9

[27] Mouhsine Bellaj, Hicham Yazid, Khalid Aziz, Abdelmajid Regti, Mohammadine El Haddad, Mounir El Achaby, Abdelkrim Abourriche, Lhoucine Gebrati, Tonni Agustiono Kurniawan, Faissal Aziz, Eco-friendly synthesis of clay-chitosan composite for efficient removal of alizarin red S dye from wastewater: A comprehensive experimental and theoretical investigation, *Environmental Research*, 247, (2024), 118352 https://doi.org/10.1016/j.envres.2024.118352

[28] Ahmed Saud Abdulhameed, AbdulKarim-Talaq Mohammad, Ali H. Jawad, Modeling and mechanism of reactive orange 16 dye adsorption by chitosan-glyoxal/TiO_2 nanocomposite: application of response surface methodology, *Desalination and Water Treatment*, 164, (2019), 346-360 https://doi.org/10.5004/dwt.2019.24384

[29] Nurul Hidayah Abdullah, Azry Borhan, Noridah binti Osman, Chan Zhing Wei, Biosorption potential of chitosan-coated rubber seed shell activated carbon for the removal of Fe(II) ions and oily solution, *Materials Chemistry and Physics*, 337, (2025), 130524 https://doi.org/10.1016/j.matchemphys.2025.130524

[30] Jerosha Ifthikar, Xiang Jiao, Audrey Ngambia, Ting Wang, Aimal Khan, Ali Jawad, Qiang Xue, Lei Liu, Zhuqi Chen, Facile One-Pot Synthesis of Sustainable Carboxymethyl Chitosan – Sewage Sludge Biochar for Effective Heavy Metal Chelation and Regeneration, *Bioresource Technology*, 262, (2018), 22-31 https://doi.org/10.1016/j.biortech.2018.04.053

[31] Meijuan Zhong, Xinge Liu, Jianfeng Ma, Lili Shang, Bamboo-Activated Carbon Synthesized by One-Pot Pyrolysis and $FeCl_2$ Activation for the Removal of Cr(VI) in Aqueous Solutions, *Water*, 15, 10, (2023), 1891 https://doi.org/10.3390/w15101891

[32] Soumya Sasmal, Vaibhav V. Goud, Kaustubha Mohanty, Characterization of biomasses available in the region of North-East India for production of biofuels, *Biomass and Bioenergy*, 45, (2012), 212-220 https://doi.org/10.1016/j.biombioe.2012.06.008

[33] Oludoyin Adeseun Adigun, Vincent Olukayode Oninla, N. A. Adesola Babarinde, K. O. Oyedotun, Ncholu Manyala, Characterization of sugarcane leaf-biomass and investigation of its efficiency in removing Nickel(II), Chromium(III) and Cobalt(II) ions from polluted water, *Surfaces and Interfaces*, 20, (2020), 100621 https://doi.org/10.1016/j.surfin.2020.100621

[34] Ekta R. Raut, Monita A. Bedmohata, Archana R. Chaudhari, Comparative study of preparation and characterization of activated carbon obtained from sugarcane bagasse and rice husk by using H_3PO_4 and $ZnCl_2$, *Materials Today: Proceedings*, 66, (2022), 1875-1884 https://doi.org/10.1016/j.matpr.2022.05.413

[35] Pradip Nandanwar, Ravin Jugade, Vaishnavi Gomase, Anita Shekhawat, Apurva Bambal, Dhandayutham Saravanan, Sadanand Pandey, Chitosan-Biopolymer-Entrapped Activated Charcoal for Adsorption of Reactive Orange Dye from Aqueous Phase and CO_2 from Gaseous Phase, *Journal of Composites Science*, 7, 3, (2023), 103 https://doi.org/10.3390/jcs7030103

[36] Seungoh Jung, Minjung Jung, Juhee Yoon, Jungkyu Kim, Hyoung-Joon Jin, Hyo Won Kwak, Chitosan-derived activated carbon/chitosan composite beads for adsorptive removal of methylene blue and acid orange 7 dyes, *Reactive and Functional Polymers*, 204, (2024), 106028 https://doi.org/10.1016/j.reactfunctpolym.2024.106028

[37] Maryam Fayazi, Masoud Ghanei-Motlagh, Mohammad Ali Taher, The adsorption of basic dye (Alizarin red S) from aqueous solution onto activated carbon/ γ -Fe_2O_3 nano-composite: Kinetic and equilibrium studies, *Materials Science in Semiconductor Processing*, 40, (2015), 35-43 https://doi.org/10.1016/j.mssp.2015.06.044

[38] Sana Ijaz, Abida Kausar, Sadia Asim, Sumera Anwar, Azo dye removal using rice husk-based nanobiochar-chitosan composite: Integration of Taguchi optimization and ANN modeling, *Desalination and Water Treatment*, 324, (2025), 101550 https://doi.org/10.1016/j.dwt.2025.101550

[39] Asma S. Al-Wasidi, Ehab A. Abdelrahman, Khalil ur Rehman, Fawaz A. Saad, Alaa M. Munshi, Efficient removal of crystal violet and acid red 88 dyes from aqueous environments using easily synthesized copper ferrite nanoparticles, *Scientific Reports*, 14, 1, (2024), 29599 https://doi.org/10.1038/s41598-024-80681-y

[40] Catarina Helena Pimentel, Rubén Castro-Agra, María Sonia Freire, Diego Gómez-Díaz, Julia González-Álvarez, Adsorption of anionic wood dyes on KOH-activated carbons from *Pinus radiata* sawdust, *Biomass Conversion and Biorefinery*, 15, 5, (2025), 7603-7622 https://doi.org/10.1007/s13399-024-05587-1

[41] Karthik Rathinam, Xinwei Kou, Ralph Hobby, Stefan Panglisch, Sustainable Development of Magnetic Chitosan Core–Shell Network for the Removal of Organic Dyes from Aqueous Solutions, *Materials*, 14, 24, (2021), 7701 https://doi.org/10.3390/ma14247701

[42] Ibrahim El-Hallag, Ahmad Al-Owais, El-Sayed El-Mossalamy, Kinetic and thermodynamic investigation of the removal of alizarin red dye using silica-supported nanoscale zero-valent iron particles, *Scientific Reports*, 15, (2025), 31461 https://doi.org/10.1038/s41598-025-15233-z

[43] A. Hashem, Chukwunonso O. Aniagor, S. Farag, M. Fikry, A. A. Aly, A. Amr, Evaluation of the adsorption capacity of surfactant-modified biomass in an aqueous acid blue 193 system, *Waste Management Bulletin*, 2, 1, (2024), 172-183 https://doi.org/10.1016/j.wmb.2024.01.004

[44] Nisreen S. Ali, Noor M. Jabbar, Saja M. Alardhi, Hasan Sh Majdi, Talib M. Albayati, Adsorption of methyl violet dye onto a prepared bio-adsorbent from date seeds: isotherm, kinetics, and thermodynamic studies, *Heliyon*, 8, 8, (2022), https://doi.org/10.1016/j.heliyon.2022.e10276

[45] Rashda, Kailu Dai, Ansa Rebi, Shumaila Kiran, Zhaohui Li, Runping Han, Adsorption efficiency of alizarin red and 2,4-dichlorphenoxyacetic acid from wastewater onto chitosan and iron oxide-coated peanut husk-activated carbon: Isothermal, kinetic, and antibacterial analyses, *International Journal of Biological Macromolecules*, 319, (2025), 145504 https://doi.org/10.1016/j.ijbiomac.2025.145504

[46] Paschal Enyinnaya Ohale, Kaito Chukwudi, Julius Nnamdi Ndive, Madiebo Emeka Michael, Mathew Ndubuisi Abonyi, Monday Morgan Chukwu, Christopher Chiedozie Obi, Chijioke Elijah Onu, Chinenye Adaobi Igwegbe, Chinenye Ogochukwu Azie, Optimization of Fe_2O_3@BC-KC composite preparation for adsorption of Alizarin red S dye: Characterization, kinetics, equilibrium, and thermodynamic studies, *Results in Surfaces and Interfaces*, 13, (2023), 100157 https://doi.org/10.1016/j.rsurfi.2023.100157

[47] Mona Moheb, Ahmad M. El-Wakil, Fathi S. Awad, Highly porous activated carbon derived from the papaya plant (stems and leaves) for superior adsorption of alizarin red s and methylene blue dyes from wastewater, *RSC Advances*, 15, 1, (2025), 674-687 https://doi.org/10.1039/D4RA07957D

[48] M. Khormaei, B. Nasernejad, M. Edrisi, T. Eslamzadeh, Copper biosorption from aqueous solutions by sour orange residue, *Journal of Hazardous Materials*, 149, 2, (2007), 269-274 https://doi.org/10.1016/j.jhazmat.2007.03.074

[49] Yao-dong Liang, Yong-jun He, Yu-hang Zhang, Qian-qian zhu, Adsorption property of alizarin red S by $NiFe_2O_4$/polyaniline magnetic composite, *Journal of Environmental Chemical Engineering*, 6, 1, (2018), 416-425 https://doi.org/10.1016/j.jece.2017.12.022

[50] S. Venkatesh, V. Arutchelvan, Biosorption of Alizarin Red dye onto immobilized biomass of *Canna indica*: isotherm, kinetics, and thermodynamic studies,

Desalination and Water Treatment, 196, (2020), 409-421 https://doi.org/10.5004/dwt.2020.25798

[51] Jiajie Zhang, Jinghua Zhang, Mengmeng Yang, Runping Han, Efficient sequestration of Alizarin red from solution using a novel adsorbent based on zirconium and diethylenetriamine functionalized wheat straw, *Desalination and Water Treatment*, 235, (2021), 283-299 https://doi.org/10.5004/dwt.2021.27624

[52] Reyhaneh Eizi, Tahereh Rohani Bastami, Vahid Mahmoudi, Ali Ayati, Hesamaddyn Babaei, Facile ultrasound-assisted synthesis of CuFe-Layered double hydroxides/g-C_3N_4 nanocomposite for alizarin red S sono-sorption, *Journal of the Taiwan Institute of Chemical Engineers*, 145, (2023), 104844 https://doi.org/10.1016/j.jtice.2023.104844

[53] Sharon Olivera, Krishna Venkatesh, Mysore Sridhar Santosh, Denis Leybo, Denis Kuznetsov, Bidarur K. Jayanna, Inamuddin, Abdullah M. Asiri, Khalid Ahmed Alamry, Handanahally Basavarajaiah Muralidhara, Open ended tube like hollow bio-carbon derived from banana fibre for removal of anionic and cationic dyes, *Desalination and Water Treatment*, 132, (2018), 297-306 https://doi.org/10.5004/dwt.2018.22932